RSC Advances

PAPER

View Article Online
View Journal | View Issue

Cite this: *RSC Adv.*, 2016, **6**, 86918

Hybrid paper–TiO_2 coupled with a Cu_2O heterojunction: an efficient photocatalyst under sun-light irradiation

Mouheb Sboui,[a] Soraa Bouattour,[a] Michelangelo Gruttadauria,[b] Leonarda Francesca Liotta,[c] Valeria La Parola[c] and Sami Boufi*[d]

Hybrid paper–TiO_2, paper–Cu_2O–TiO_2 and paper–TiO_2–Cu_2O photocatalysts were prepared *via* a non-hydrolytic sol–gel process followed by mild hydrothermal treatment to generate the TiO_2 layer, and a reduction process to form the Cu_2O nanoparticles. The hybrid photocatalysts have been characterized by Raman, TGA, FE-SEM, UV-Vis and XPS. The immobilized TiO_2 was found to form a homogeneous thin layer composed of nanoparticles with a size smaller than 10 nm. The Cu_2O nanoparticles with sizes of 30–100 nm were generated either on the top of the TiO_2 layer or by reduction of Cu^{2+} ions. All the prepared hybrid catalysts showed efficient photocatalytic properties for the degradation of toluidine when exposed to simulant solar light. A strong enhancement in the photocatalytic activity was observed when TiO_2 was coupled with the Cu_2O heterojunction, with the highest effect being observed when the Cu_2O NPs were present on top of the TiO_2 layer. The hybrid photocatalyst can be reused for at least four consecutive cycles without a significant decrease in the degradation efficiency. The preparation technique of the hybrid catalyst is reliable, economic, easy to implement and may be scaled to prepare paper–TiO_2 hybrid photocatalysts active under sun-light exposure.

Received 11th August 2016
Accepted 6th September 2016

DOI: 10.1039/c6ra20248a

www.rsc.org/advances

1. Introduction

TiO_2–anatase is one of the most studied and efficient photocatalysts for the decomposition of a wide range of organic pollutants, as it transforms them into inorganic or readily biodegradable organic species. However, despite the recognized advantages of TiO_2, including chemical and biological inertness, cost-effectiveness and wide possibility of chemical modification, the scale-up use in real water treatment and environmental remediation is still limited and below expectations. One major obstacle is related to the recovery and recycling of the powdered titania photocatalyst when used in slurry. The necessity of UV-light to activate TiO_2 (due to the band gap around 3.2 eV for anatase) and the fast recombination rate of the photogenerated electron/hole pairs are two other shortcomings of TiO_2 that have hampered its widespread development.

The immobilization of TiO_2 onto an inert support is a convenient method to overcome the problem of powder filtration and recovery of the catalyst. It also offers flexibility in the photocatalyst handling and its use for air or water purification systems. Examples of inert supports include glass fibres, glass rods[1,2] or beads,[3] carbon,[4] cotton,[5] metal, carbon cloth[2] or membranes.[6]

Paper–TiO_2 hybrid nanostructures have received considerable attention because they integrate both benefits of paper and TiO_2 in a single high performance material. The main paper benefits include lightness, flexibility, and availability in a wide range of thickness and the specific attributes of TiO_2 include photocatalytic, electronic, optical and antibacterial properties.[7] Moreover, the particular structure of cellulose with a multitude of surface hydroxyl groups favours the adhesion between TiO_2 and the surface of fibres through cellulose–O–Ti bridging, as was reported in the literature.[8] This structure offers an excellent template for the nucleation of nanostructured TiO_2. The two main applications of paper–TiO_2 photocatalyst are the degradation of organic pollutants, including dyes and volatile organic compounds (VOC), disinfection and deodorization of the surrounding air.

The first work demonstrating the photocatalytic activity of paper–TiO_2 was reported by Matsubara *et al.*[9] in 1995 describing the preparation of composite catalyst and their use to decompose acetaldehyde in vapour phase under weak fluorescent light illumination. Then, Tanaka and co-workers[10] prepared several types of photocatalytic paper composites with a dual polymeric retention system, using TiO_2 supported on the cellulose fibers. The papers were found to be effective for the removal of bisphenol from wastewater and acetaldehyde and toluene from

[a]*University of Sfax, Faculty of Science, LCI, BP1171-3018 Sfax, Tunisia*
[b]*Dipartimento Scienze e Tecnologie Biologiche, Chimiche e Farmaceutiche (STEBICEF), Università degli Studi di Palermo, Viale delle Scienze, Ed. 17, 90128 Palermo, Italy*
[c]*Istituto per lo Studio dei Materiali Nanostrutturati, ISMN-CNR, Via Ugo La Malfa 153, 90146-Palermo, Italy*
[d]*University of Sfax, Faculty of Science, LSME, BP1171-3018 Sfax, Tunisia. E-mail: Sami.Boufi@fss.rnu.tn*

indoor air. Uddin *et al.*[7] reported an original approach for the immobilization and grafting of TiO_2 on cellulose fibers using a sol–gel method at low temperature. Homogeneous thin film, composed of TiO_2 nanoparticles 3–5 nm in size, was generated on the surface of the paper and the photocatalytic activity was demonstrated by the degradation of methylene blue under solar-like light exposition.

Another chemical approach aiming to better control the chemical anchoring of TiO_2 on paper was proposed by Kemell *et al.*[11] This approach is based on the vapour phase treatment of $Ti(OMe)_4$ in the presence of water vapour, giving 30–50 nm-thick film of amorphous TiO_2.[11] It was reported that TiO_2 could be turned into a photoactive form, while maintaining the paper structure by annealing at 250 °C. A good review providing an overview of the developing field of photocatalytic papers was reported by Pelton *et al.*[12]

Currently two approaches are used for adding a photocatalyst to the paper during the papermaking process. The first one is the wet-end addition where TiO_2 is mixed with the paper mill suspension and filtered together during the sheet formation. However, only a fraction of TiO_2 particles can be included in the paper-web and nano-sized TiO_2 cannot be used because of aggregation problems. Moreover, only a fraction of TiO_2 can be accessible on the top surface of the paper, thus limiting the photocatalytic activity. The second approach is the coating of TiO_2 on the dry paper using the size press during which where the dry paper sheet is impregnated with a suspension TiO_2 by passing through two-roll press followed by a drying treatment. However, a binder is often necessary to firmly bond the pigment particles together and to the underlying paper. Moreover, the presence of the polymer layer and other processing additives are likely to impair the photocatalytic activity of TiO_2. Therefore, there is a need to look on a more effectively approach to immobilize in a controlled way on paper a nanosized layer of TiO_2 without impairing the flexibility of paper nor its thermal or chemical stability. One possibility is to generate the TiO_2 layer *via* the sol–gel method starting from the conventional $Ti(OBu)_4$ precursor. Another possibility is the is the direct adsorption of ready-made titania nanoparticles (TiO_2 sol) onto paper followed by a mild thermal treatment to promote the irreversible anchoring of the TiO_2 NPs onto the surface of fibres.

Besides, to extend the light absorption properties of TiO_2 and drive the photocatalytic activity to visible light, the coupling of TiO_2 with a narrow band gap semiconductor such as Cu_2O can be considered. In fact Cu_2O aroused increasing interest for different reasons: (i) Cu_2O has a low band gap at 2.2 eV which makes it a potential sensitizer for TiO_2 under visible light irradiation,[13] (ii) the conduction band of Cu_2O is located at a more negative level than the conduction band potential of TiO_2, thus thermodynamically favoring the electron transfer from Cu_2O to TiO_2,[14] (iii) the heterojonction Cu_2O/TiO_2 favors the transfer of photoexcited electrons and holes between them, which is beneficial for improving the photocatalytic performance, (iv) Cu_2O is easy to synthesize with various morphologies that can influence its activity, including nanowires, spheres, cubes, octahedral, truncated octahedral and so on.[15] For these reasons, it is interesting to investigate how the coupling of Cu_2O with TiO_2 immobilized on paper is likely to affect the photocatalytic properties of hybrid paper–TiO_2, especially that no data has been reported on the literature concerning paper–TiO_2–Cu_2O composite photocatalyst.

In the present work, a novel approach for the coating of paper with a nanosized layer of TiO_2 decorated with Cu_2O NPs, through a cost effective and green chemistry process using mild conditions, is described. TiO_2 NPs were generated directly onto the sheet paper *via* a non-hydrolytic sol–gel approach using $Ti(OBu)_4$ as a precursor, followed by a mild hydrothermal treatment. The Cu_2O NPs were formed either prior to the treatment with $Ti(OBu)_4$ or after growth of TiO_2 layer. The prepared hybrid paper–TiO_2, paper–Cu_2O–TiO_2 and paper–TiO_2–Cu_2O were characterized by Raman, TGA, FE-SEM, UV-Vis and XPS. The photocatalytic activity was evaluated for the degradation of toluidine as an aromatic amine model pollutant.

2. Experimental

2.1. Materials

All chemical reagents provided by Aldrich were of analytical grade and used without further purification, including $Ti(OBu)_4$, glacial acetic acid, *tert*-butanol 99.7% purity, $CuSO_4$, hydrazine monohydrate ($NH_2NH_2 \cdot H_2O$), NaOH and HCl commercial parchment (with a cellulose content exceeding 99%) was provided from SOTEFI Industry (Tunisia).

2.2. Fabrication of TiO_2–Cu_2O/cellulose paper

The paper were first dried at 70 °C for 2 h to remove adsorbed water and immediately dipped into a 1 (w/v)% solution of $Ti(OBu)_4$ in a mixture of *tert*-butanol and acetic acid (90/10 wt%) for 2 h. Samples were then removed and dried at 60 °C for 2 h in an oven to evaporate the solvent and then autoclaved in a Teflon-lined autoclave at 120 °C for the hydrothermal treatment during 3 h. Finally, samples were allowed to dry in an oven at 60 °C for 3 h before characterisation.

Cu_2O nanoparticles were loaded on paper–TiO_2 by a simple immersion process in a solution of $CuSO_4$ in water followed by a reduction with hydrazine at room temperature. For paper–Cu_2O–TiO_2, the paper was first soaked in a solution of $CuSO_4$ at a pH = 5.5 for 2 h. Then, the paper was removed from the solution, rinsed with water two times, and then immersed in an aqueous solution of hydrazine monohydrate ($NH_2NH_2 \cdot H_2O$) (650 μL in 20 mL distilled water) kept at pH = 12 by the addition of NaOH solution.

For paper–TiO_2–Cu_2O the same procedure was applied using paper–TiO_2 instead of neat paper. The synthesis approaches adopted for the preparation of paper–TiO_2, paper–TiO_2–Cu_2O and paper–Cu_2O–TiO_2 are depicted in Scheme 1.

2.3. Photocatalytic activity

The photcatalytic degradation tests were performed as follows: paper sample 4 × 4 cm was introduced in 50 mL solution of toluidine (5×10^{-4} mol L^{-1}) kept in an open glass flask with 50 mm in diameter. Before irradiation, solutions were maintained in the dark for one hour. The system was then illuminated by

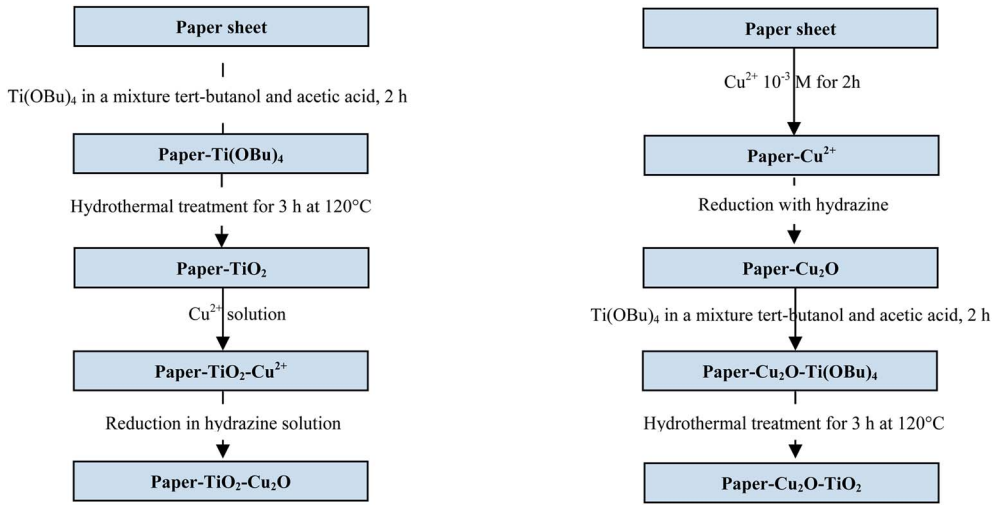

Scheme 1 Illustration of the different steps adopted to prepare paper–TiO_2 hybrid material.

a 50 W xenon lamp placed at 10 cm from the top of the beaker. At constant time intervals, 1 mL aliquots were sampled and then analyzed on a Cecil UV-visible spectrophotometer. The UV absorbance of TD solution was measured at 235 nm and the concentration was determined from the corresponding calibration curve. The photocatalytic activity was expressed in the percentages of toluidine degradation according to the following equation (eqn (1)):

$$\text{Degradation} = C_t/C_0 \times 100 \text{ (in \%)} \quad (1)$$

where C_0 is the initial concentration at time $t = 0$, and C_t is the concentration at time interval.

At the end of every cycle, the sample was washed with distilled water and then dried for the next cycle. All photocatalytic tests were performed under the same experimental conditions.

2.4. Raman spectra

Raman spectra were recorded on a LabRAM Analytical Raman micro-spectrograph (Jobin–Yvon, Horiba group, France) using a He–Ne laser source as exciting radiation ($\lambda = 632.8$ nm) and an air cooled CDD detector. The acquisition time was 100 s.

2.5. Thermogravimetric analysis (TGA)

The thermogravimetric analysis was performed using a TGA 400 Perkin Elmer. The paper sample was heated from 25 °C to 800 °C at a rate of 10 °C min^{-1} under air flow.

2.6. UV-vis spectra

Ultraviolet-visible (UV-vis) spectra of samples were collected on a spectrophotometer (Perkin Elmer Lambda 35). The UV-vis spectra have been obtained in the reflectance mode on the dried samples. The reflectance R was obtained from each sample in the UV-vis spectral regions and the remission function $F(R)$ was calculated using the Kubelka–Munk equation for optically thick samples. The remission function is $F(R) = (1 - R)^2/2R$.

2.7. XPS analysis

The X-ray photoelectron spectroscopy analyses were performed with a VG Microtech ESCA 3000Multilab, equipped with a dual Mg/Al anode. The spectra were excited by the unmonochromatized Al Kα source (1486.7 eV) run at 14 kV and 15 mA. The analyser operated in the constant analyser energy (CAE) mode. For the individual peak energy regions, a pass energy of 20 eV set across the hemispheres was used. Survey spectra were measured at 50 eV pass energy. The sample powders were analysed mounted on a double-sided adhesive tape. The pressure in the analysis chamber was in the range of 10^{-8} Torr during data collection. The constant charging of the samples was removed by referencing all the energies to the C 1s set at 285.1 eV, arising from the adventitious carbon. The invariance of the peak shapes and widths at the beginning and at the end of the analyses ensured the absence of differential charging. Analyses of the peaks were performed with the software provided by VG based on non-linear least squares fitting program using a weighted sum of Lorentzian and Gaussian component curves after background subtraction according to Shirley and Sherwood.[16] Atomic concentrations were calculated from peak intensity using the sensitivity factors provided by the software. The binding energy values are quoted with a precision of ± 0.15 eV and the atomic percentage with a precision of $\pm 10\%$.

3. Results and discussion

3.1. Raman characterization

Raman spectroscopy is known to be more sensitive to shorter range order than XRD and constitutes a powerful method to probe the microstructure of nanoparticles, namely for TiO_2 materials. Furthermore, both cellulose and TiO_2 phases are active in Raman, making possible to get an indication about the

relative proportions between the two phases. Raman spectra of neat paper, paper–TiO_2, paper–TiO_2–Cu_2O and paper–Cu_2O–TiO_2 are given in Fig. 1. The neat paper is characterized by the typical bands of cellulose at 376, 432, 454, 515, 1094 and 1116 cm^{-1}. The most intense bands at 1094 and 1116 cm^{-1} are assigned to the C–O–C (symmetric and asymmetric) stretching mode of the β (1-4) glycosidic bonds of the glucopyranose ring of cellulose. In the paper–TiO_2 new bands at 147 cm^{-1}, 519 cm^{-1} and 637 cm^{-1} emerged in addition to the bands of paper only. These bands are typical of TiO_2 anatase and were assigned to the vibrational modes of anatase phase corresponding to the E_g (low-frequency, stretching vibration of O–Ti–O in TiO_2) and E_g (high frequency).[17,18] The presence of these peaks gave a sound evidence of the formation of crystalline anatase bound to the surface of the paper *via* the mild approach adopted. Although, only a mild hydrothermal treatment at 120 °C was carried out for the paper after contact with the $Ti(OBu)_4$ solution in *tert*-butanol, a successful crystallisation of TiO_2 on the surface of the paper took place. As we have explained in our previous work,[4] the unusual low temperature of TiO_2 crystallization was explained by the low thickness of the TiO_2 layer and by the controlled hydrolysis of $Ti(OBu)_4$ precursor during the contact between paper and the solution of the precursor. During the hydrothermal treatment, the butoxy groups are progressively hydrolyzed into Ti–OH and rapidly underwent condensation *via* olation/oxolation with the progressive nucleation and growth of thin TiO_2 layer. For paper–TiO_2–Cu_2O and paper–Cu_2O–TiO_2 samples, a new band at 218 cm^{-1} typical of Cu_2O was visible in the spectrum in addition to bands of cellulose and TiO_2 which confirmed the presence of Cu_2O phase with TiO_2 anatase.

3.2. Contact angle measurement

The static water contact angle was analyzed to assess the wetting properties of the hybrid photocatalyst. The technique is based on the observation of a small liquid drop on the surface *vs.* time.

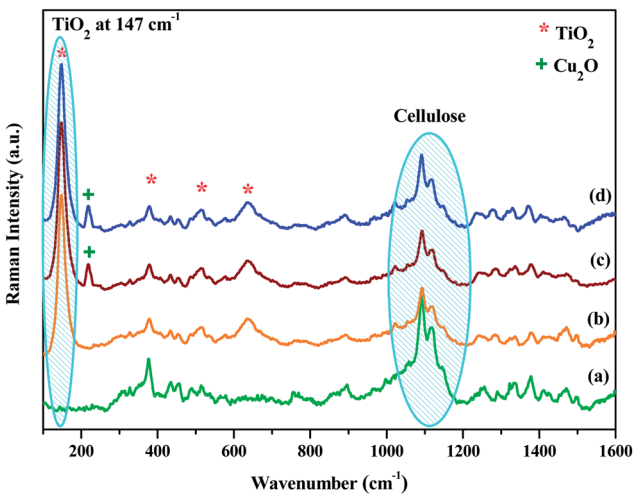

Fig. 1 Raman spectra of: (a) neat paper, (b) paper–TiO_2, (c) paper–TiO_2–Cu_2O and (d) Paper–Cu_2O–TiO_2.

The neat paper exhibited a hydrophobic surface with a contact angle around 120° (Fig. 2). This hydrophobic character may be explained by the particular structure of the paper used and the way used to produce this paper. Actually, the paper used was commercial parchment paper made by passing sheet of paper for a few seconds in sulfuric acid, followed by several washes in water. During this process, fibers partially gelatinize, filling the interstices between the fibers and resulting in extensive hydrogen bonding. The porosity of paper, responsible for water absorption, was removed and paper become water proof and well consolidated. The absence of porosity and the particular surface morphology accounts for the hydrophobic surface of the paper as attested by the contact angle around 120°. After generation of the TiO_2 layer, the paper–TiO_2 hybrid material turned to hydrophilic with a contact angle around 40°. This hydrophilic character is presumably the result of the presence of surface Ti–OH groups formed following the hydrothermal treatment. The same stands for paper–Cu_2O–TiO_2 with a contact angle around 47°. On the other hand, paper–TiO_2–Cu_2O is again hydrophobic with a contact angle around 110°. Two reasons may account for the hydrophobic surface of paper–TiO_2–Cu_2O. The first one is the vanishing of the surface hydroxyl groups on TiO_2 masked by the Cu_2O NPs on which they grow. This occurs because of the preferential adsorption of Cu^{2+} on the Ti–OH group prior to the reduction process. The second reason is the surface morphology made up with tiny nanosized grains which contributed to generate microroughness that further increases the hydrophobicity by decreasing the contact area between water and the surface protrusion of Cu_2O NPs as clearly seen in the SEM observation.

It is worth to note that the hydrophobic character is beneficial for the photocatalyst since it prevents the disintegration of the paper support when being in contact with water and it gives a self-cleaning property to the catalyst by preventing the adhesion of the by-product generated during the degradation process.

3.3. Thermal behavior

The thermal behaviour of neat paper, paper–TiO_2, paper–Cu_2O–TiO_2 and paper–TiO_2–Cu_2O samples was studied by thermogravimetric analysis (TGA) under air flow (Fig. 3). Three steps of degradation are seen in all of the samples. The first one, with a loss of about 5%, occurs in the range of 75–150 °C, and is attributed to the evaporation of water bound to fibers. The second one, starting at 250 °C and extending up to 350 °C, is attributed to the degradation of the saccharide backbone by the cleavage of the glycosidic bond, the depolymerization and the dehydration of saccharide rings. The third step is observed between 360 °C and 560 °C and is ascribed to the complete oxidative degradation of the carbonaceous residue formed during the second step. The final residual mass, after heating at 600 °C, was about 6, 8, 8.9 and 10% 1.5, 2 and 2.5% for neat paper, paper–TiO_2 and paper–Cu_2O–TiO_2, respectively. The weight fraction of the generated TiO_2 and Cu_2O (with respect to the paper) for the different samples could be estimated to about 1.6, 2.5 and 3.9% for paper–TiO_2 and paper–Cu_2O–TiO_2 paper–TiO_2–Cu_2O, respectively. The low residual chart after complete degradation is the consequence

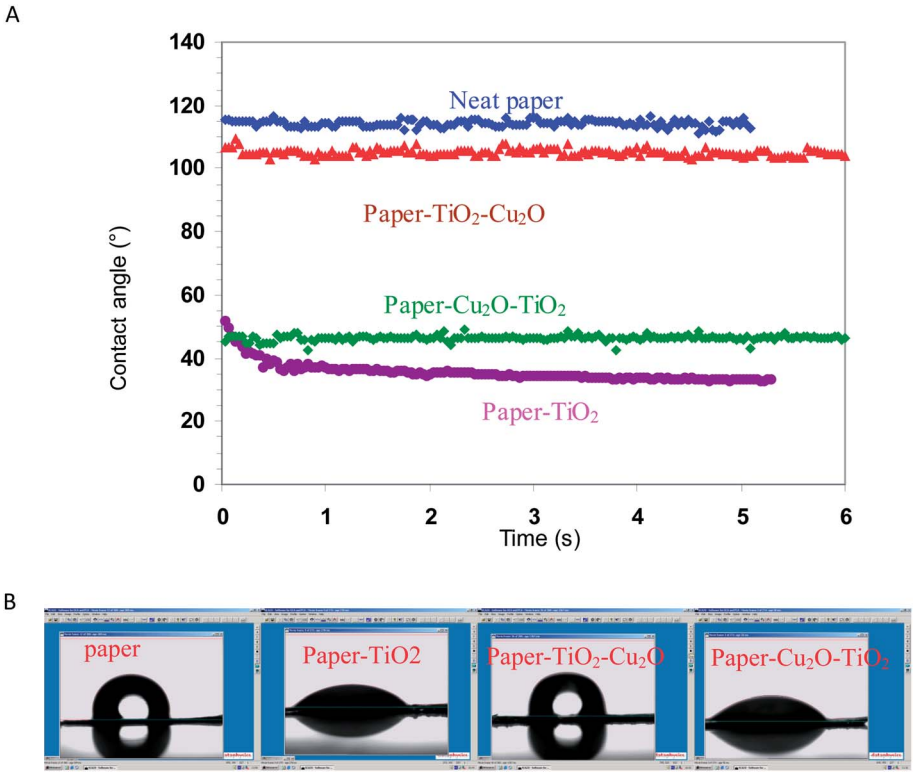

Fig. 2 (A) Water contact angle changes on paper and hybrid paper–TiO_2, paper–Cu_2O–TiO_2 and paper–TiO_2–Cu_2O, and (B) the captured micrographs of water droplet on the corresponding surface.

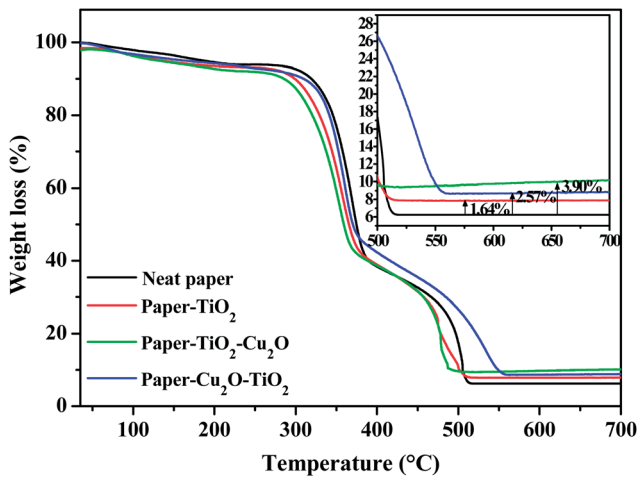

Fig. 3 Weight loss (%) as a function of the increasing temperature (with constant heating rate) for four different samples: neat paper, paper–TiO_2, paper–TiO_2–Cu_2O and paper–Cu_2O–TiO_2.

of the low thickness of the generated TiO_2 layer, which based on FE-SEM observation did not exceed about 50 nm. Moreover, neither TiO_2 nor Cu_2O seems to meaningfully alter the thermal stability of the paper which appears stable up to 280 °C.

3.4. SEM observation

The FE-SEM images of the neat paper prior and after functionalization with TiO_2 are shown in Fig. 4. Observations of the structure of paper at higher magnification revealed the different levels of organization of the paper. It can be seen that the paper has a closed surface structure without any porosity and is made of layered fibrous network structure with in plane random orientation of fibers. These later were flattened, well mutually bounded and seem to be welded together, which is the consequence of the preparation method of paper by rapid passing in a sulfuric acid. As highlighted above, the absence of any porosity along with the close layered structure of the paper contributed to reinforce the paper strength. At higher magnification, further details of the complex ultra structure of the cellulose fibers can be seen, revealing the nanosized cellulose fibrils composing the cellulose fibers.

After functionalizing the paper with TiO_2 (Fig. 4B), no visible change was observed on the surface morphology and on the aspect of fibers, since the magnification factor was lower than 2000, which is indicative of the lower thickness of the layer. A magnification over 10 000 is needed in order to see details on the change occurring after the different treatments. For paper–TiO_2, the elementary cellulose nanofibrils were no longer visible revealing the existence of a continuous thin layer of titanium oxide covering the cellulosic surface composed of tiny nanoparticles with a size around 10 nm. For paper–Cu_2O–TiO_2, the same trend was noted with the difference that protrusions were evenly observed along the TiO_2 layer, which presumably corresponds to Cu_2O NPs underneath the layer of TiO_2. In order to confirm that Cu_2O NPs were generated during the first step prior to the coating with $Ti(OBu)_4$ precursor, SEM observation

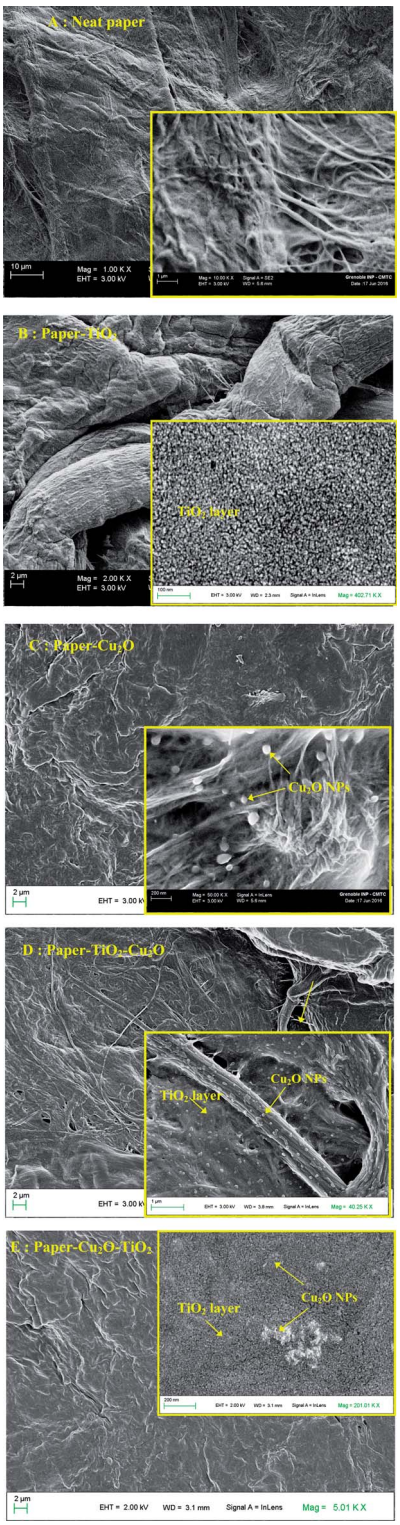

Fig. 4 FE-SEM images of neat; paper (A) paper–TiO_2, (B) paper–Cu_2O, (C) paper–TiO_2–Cu_2O, (D) and paper–Cu_2O–TiO_2 (E).

was carried out on paper immersed successively in a solution of Cu^{2+} and hydrazine for reduction. Image in Fig. 4B revealed the formation of NPs with about 30 to 100 nm well bounded to the cellulose fibrils. This methodology was based from our previous work for the functionalization of cotton fibers with Cu_2O NPs.[19]

A different surface morphology was noted for paper–TiO_2–Cu_2O. The surface of the paper showed at high magnification a continuous layer with similar aspect as seen for paper–TiO_2 and presumably corresponding to the TiO_2 layer over which were attached NPs having spherical to stretched form and size in the range of 30 to 100 nm in width corresponding presumably to Cu_2O generated after the growth of the TiO_2 layer. The surface distribution of Cu_2O NPs looks denser than when Cu_2O was first generated on paper. The higher capacity of Cu^{2+} ions to adsorb on TiO_2 layer at pH 5 during the adsorption step may be a reason for the higher surface density.

3.5. UV-vis characterization

The Ground State Diffuse Reflectance (GSDR) spectra for neat paper, paper–TiO_2, paper–Cu_2O–Ti_2O and paper–TiO_2–Cu_2O were shown in Fig. 5. The diffuse reflectance measurements were converted into the equivalent absorption coefficient using the Kubelka–Munk method $F(R) = (1 - R)^2/2R = \alpha$.[20] The untreated paper presents no absorption bands above 275 nm, which is consistent with the absorption spectrum of a pure cellulose sample. The paper–TiO_2 exhibited no absorption in the visible domain with absorption edge around 380 nm, which is in agreement with literature data. On the other hand, for paper–Cu_2O–TiO_2 and paper–TiO_2–Cu_2O samples, the absorption has shifted into the visible extending up to 500 nm. The red shift in the absorption is the consequence of the presence of Cu_2O phase with a strong absorption between 300 to 600 nm. However, the red shift in the absorption was more prominent for paper–TiO_2–Cu_2O than paper–Cu_2O–TiO_2. This means that the contribution to the light absorption by Cu_2O was higher when Cu_2O phase was deposited on TiO_2 layer and not underneath. The extended absorbance of paper–TiO_2–Cu_2O composite photocatalysts in the visible range is expected to improve the photocatalytic activities of Cu_2O/TiO_2 p–n heterojunction particles under visible light.

The band gap values of paper–TiO_2, paper–Cu_2O–TiO_2 and paper–TiO_2–Cu_2O were determined by the construction of Tauc plots ($(\alpha * h\nu)^n$ *vs.* $h\nu$), $\alpha = (1 - R)^2/2R = F(R)$, where α is the optical absorption coefficient, R is the reflectance of the semiconductor, $R = 10^{-A}$, and A is the optical absorbance, $F(R)$ is the Kubelka–Munk function and, ν is light frequency. Paper–TiO_2 has a band gap 3.1 eV which is lower than the value (*ca.* 3.2 eV) reported for pure anatase. However, lower value was also reported by Wu and Qi[21] for thin TiO_2 films (Table 1). In the presence of Cu_2O, a decrease in the band gap to 2.1–2.4 eV was noted, which is attributed to the intrinsic properties of Cu_2O. These values are in agreement with literature data for TiO_2–Cu_2O composites.[22] However, when Cu_2O was underneath the TiO_2 layer, the band gap was higher than that of Cu_2O (Table 1).

3.6. XPS characterization

The XPS characterization was carried out over three samples: the neat paper, the paper–TiO_2 and the paper–TiO_2–Cu_2O. The latter one was selected being more active than the paper–Cu_2O–TiO_2. The analysis shows that the synthetic procedure efficiently covers the surface of the substrate by TiO_2 as

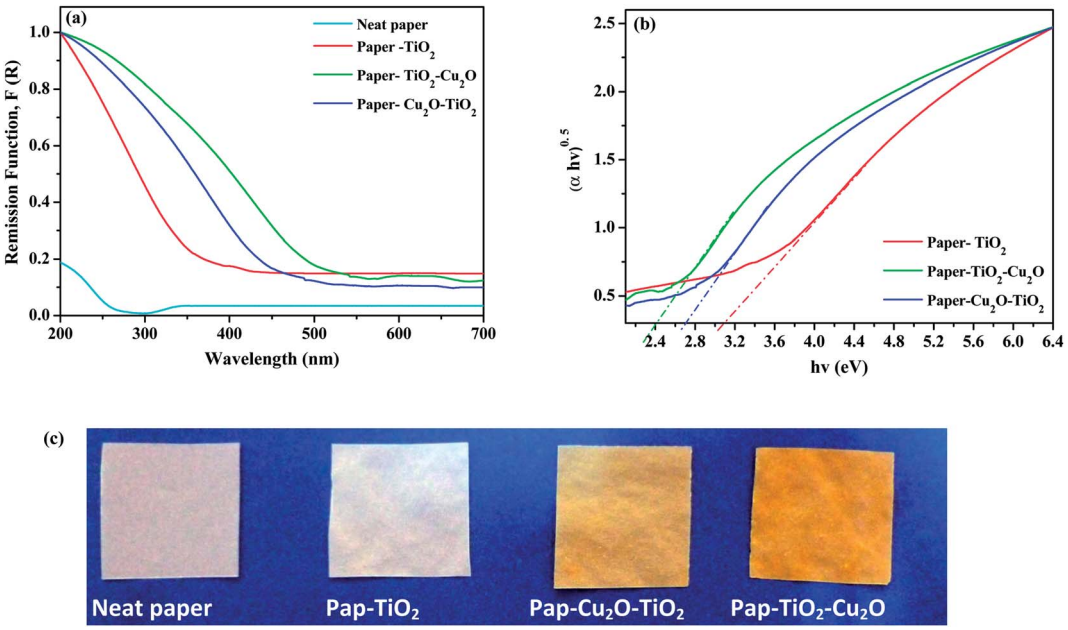

Fig. 5 (a) Ground State Diffuse Reflectance (GSDR) spectra of neat paper, paper–TiO_2, paper–TiO_2–Cu_2O and paper–Cu_2O–TiO_2. (b) Tauc plots ($(\alpha^*h\nu)^n$ *vs.* $h\nu$) constructed from panel (a), and (c) digital photos of hybrid paper photocatalyst.

Table 1 Energy gaps, λ_{max} for neat paper, paper–TiO_2, paper–Cu_2O–TiO_2, and paper–TiO_2–Cu_2O

	λ_{abs} (nm)	E_{gap} (eV)
Paper–TiO_2	380	3.1
Paper–Cu_2O–TiO_2	450	2.4
Paper–TiO_2–Cu_2O	500	2.15

evidenced by the analysis of the survey showed in Fig. 6a. By looking at the spectra a disappearance of Si peaks present in the paper, the appearance of all the peaks due to titanium and a downshift of the O 1s peak form 533 eV of the bare paper to *ca.* 530 eV typical of TiO_2 materials can be seen. Both the Ti 2p at 458.8 eV and O 1s at 529.9 eV and 531.5 eV peaks positions are typical of TiO_2.

The XPS survey scan spectra of, paper–TiO_2–Cu_2O and paper–Cu_2O–TiO_2 are shown in Fig. 6b. Besides the peaks due to TiO_2 whose positions are the same as paper–TiO_2, the peaks due to the Cu element, are highlighted. In Table 2 the position of the peaks, in terms of binding energy, and the Cu/Ti atomic ratio are reported. The Ti 2p peak is centred at 458.8 eV, while for Cu $2p_{3/2}$ the peak is centred at 932.3 eV. The peak position of Cu and the lack of the shake up features are indicative of the presence of Cu_2O.[23,24] Furthermore, the absence of the multiplet structure, between 938 and 947 eV, typical of Cu^{2+} species is a further confirmation of the total reduction of Cu^{2+} to Cu^{+} after treatment with hydrazine.[18] In paper–Cu_2O–TiO_2 sample the Cu $2p_{3/2}$ peak was not visible in XPS, presumably because Cu_2O NPs have been covered by the TiO_2 layer with thickness exceeding the analysis depth of XPS being around 8–10 nm.

3.7. Photodegradation of toluidine

To investigate the photocatalytic activity of the composite paper catalysts, the photocatalytic degradation of toluidine as a model of aromatic amine, has been conducted in water and under simulated sunlight irradiation. Prior to irradiation, the set-up was stored in the dark for 1 h to discard any possible change in the solute concentration resulting from the adsorption process. The residual concentration of toluidine was then followed by UV-Vis spectroscopy by measuring the absorbance at λ_{max}. The studies were carried out at a toluidine initial concentration ranging from 10 to 50 mg L^{-1}. The pH value ranges from 3 to 12 (for this section, the concentration of the solution is 25 mg L^{-1}). The results are shown in Fig. 7 and 8.

Before being exposed to light irradiation, the adsorbed amount of toluidine did not exceed 5%, for paper–TiO_2 neither for paper–Cu_2O–TiO_2 nor for paper–TiO_2–Cu_2O, that is indicative of the low adsorption capacity of the paper–TiO_2 hybrid material. The change in the concentration of toluidine under irradiation was negligible in the presence of neat paper, which confirmed the effective role of the TiO_2 nanolayer in the photocatalytic activity. In presence of the paper functionalized with TiO_2 and after exposure to simulated sunlight, the concentration of the toluidine progressively decreased. However, the magnitude of the decrease in the concentration of the toluidine is much more pronounced when Cu_2O was present, either underneath or on the top of the TiO_2 layer. For instance, using a sample of treated fabric 4 × 4 cm^2 in 50 mL solution of toluidine (25 mg L^{-1}), the residual concentration of toluidine was about 70, 25 and 7%, for paper–TiO_2, paper–Cu_2O–TiO_2 and paper–TiO_2–Cu_2O respectively after exposure of the solution during 6 h to simulated sunlight (Fig. 7). Assuming a first-order kinetic of the degradation process, the rate-constant values were calculated (see Table 3). The k value for

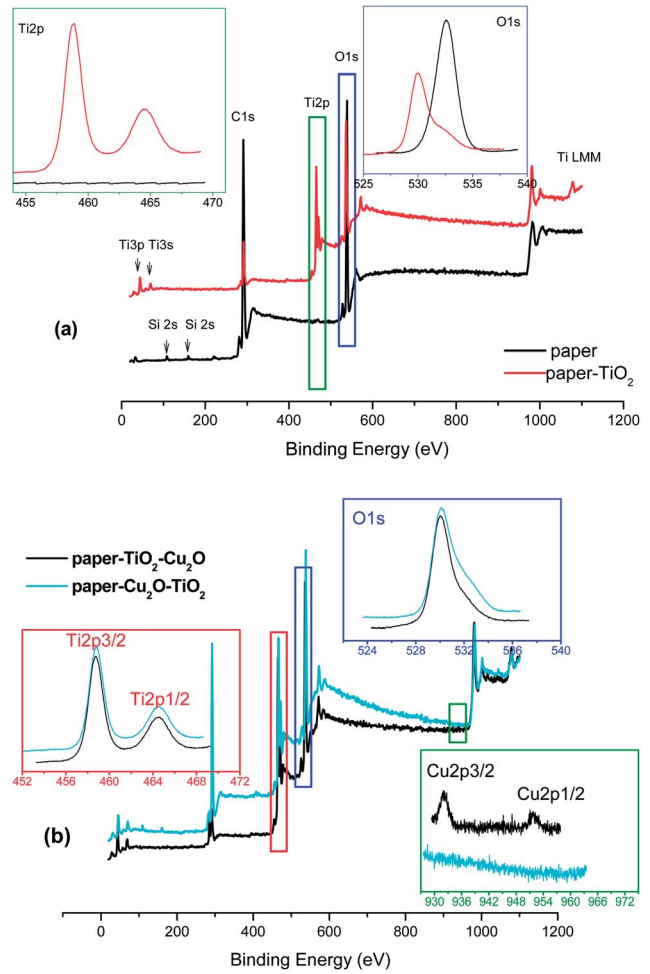

Fig. 6 (a) XPS survey of paper and paper–TiO_2; (b) XPS survey of paper–TiO_2–Cu_2O and paper–Cu_2O–TiO_2. In the inset the high resolution O 2s and Ti 2p and Cu 2p regions are reported.

paper–Cu_2O–TiO_2 and paper–TiO_2–Cu_2O was about 3 and 5 times higher than that of paper–TiO_2, confirming the strong beneficial role of Cu_2O in enhancing the photocatalytic activity under sunlight. However, when Cu_2O was on the top of the TiO_2 layer, the photocatalytic activity seems to be higher than when it was underneath. It is likely that the burying of Cu_2O under TiO_2 may reduce the contribution of copper oxide nanoparticles to the photodegradation process. The effect of pH on the degradation kinetic was also investigated by comparing the residual concentration of toluidine after exposure during 300 min to sunlight simulator. Results shown in Fig. 8 indicated a decrease in the photocatalytic efficiency under acid pH. The degradation rate was about 80, 85 and 90% at pH 3, 5 and 7, respectively. This evolution may be explained by the evolution of the surface charge of TiO_2 and the protonation of toluidine according to pH values.

Assuming the IEP (isolectric point) of TiO_2 to be in the range of 5–6 and the pK_a of toluidine around 4.5, then at pH lower than 4, the surface of TiO_2 is postively charged and the toluidine is protonated. Accordingly, the adsorption of toluidine on the surface of TiO_2 is disfavoured at acid pH, while over pH 7, the amine function of toluidine is no longer protonated and the adsorption becomes favoured.

Table 2 XPS Ti 2p, O 1s and Cu $2p_{3/2}$ binding energies (eV) along with O/Ti and Cu/Ti atomic ratios. The relative percentages of O 1s components are given in parentheses

	Ti $2p_{3/2}$	O 1s	Cu $2p_{3/2}$	O/Ti	Cu/Ti
Paper		533.0 (100)			
Paper–TiO_2	458.8	529.9 (70) 531.9 (30)		2.98	
Paper–TiO_2–Cu_2O	458.8	530.0 (70) 531.5 (30)	932.3	2.76	0.01
Paper–Cu_2O–TiO_2	458.8	530.0 (65) 531.7 (35)	n.r.	3.0	n.r.

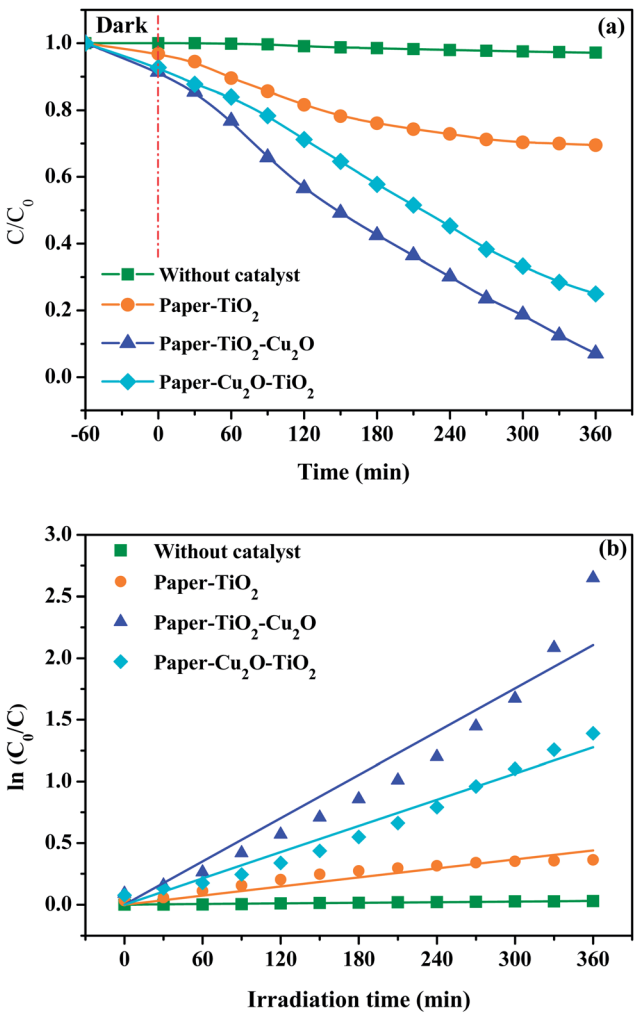

Fig. 7 (a) Time dependence of the relative concentration of toluidine upon light exposure to sunlight simulator and (b) the kinetic plot in presence of: neat paper; paper–TiO_2; paper–TiO_2–Cu_2O; paper–Cu_2O–TiO_2.

The effect of the amount of Cu_2O generated on the TiO_2 layer was studied by changing the initial concentration of the Cu^{2+} solution where the paper–TiO_2 was immersed before the reduction process. Since the adsorbed amount of Cu^{2+} ions on the surface of paper–TiO_2 is related to the initial concentration of Cu^{2+}, then the amount of Cu_2O can be tuned by the initial

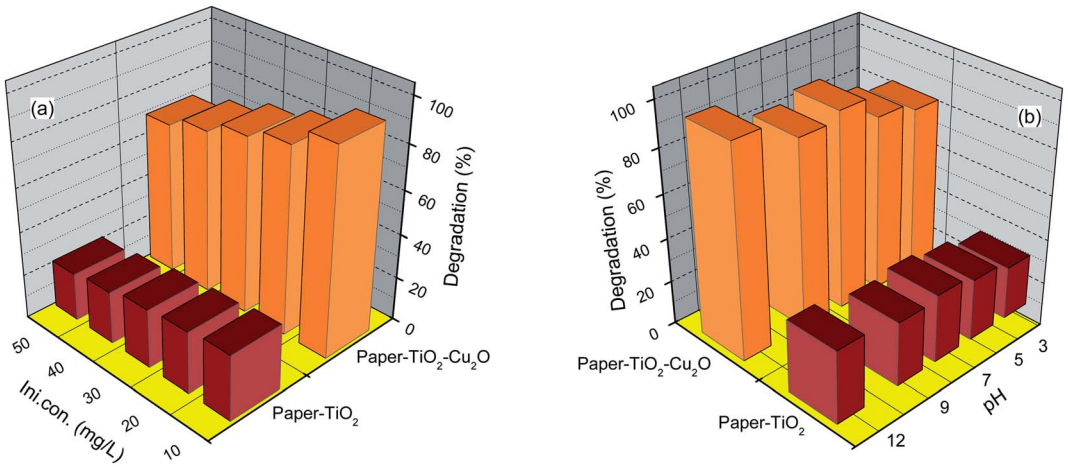

Fig. 8 (a) Effect of initial concentration on the photodegradation of toluidine after 5 h. (b) Effect of pH values on the photodegradation of toluidine.

Table 3 k and R^2 calculated for the photodegradation of toluidine over different catalysts

	Kinetic constant (k h^{-1})	R^2
Without catalyst	8.15127×10^{-5}	0.990
Paper–TiO_2	0.00123	0.9685
Paper–TiO_2–Cu_2O	0.00585	0.96802
Paper–Cu_2O–TiO_2	0.00355	0.98728

concentration of the Cu^{2+} precursor. The results shown in Fig. 9 indicated that the degradation efficiency increased by increasing the initial Cu^{2+} concentration up to 10^{-3} mol L^{-1}, then it falls again with further increase in the concentration of copper ions. This suggests that a critical content of Cu_2O, obtained after reduction in mild conditions of the Cu^{2+} precursor, is required for optimal photocatalytic activity.

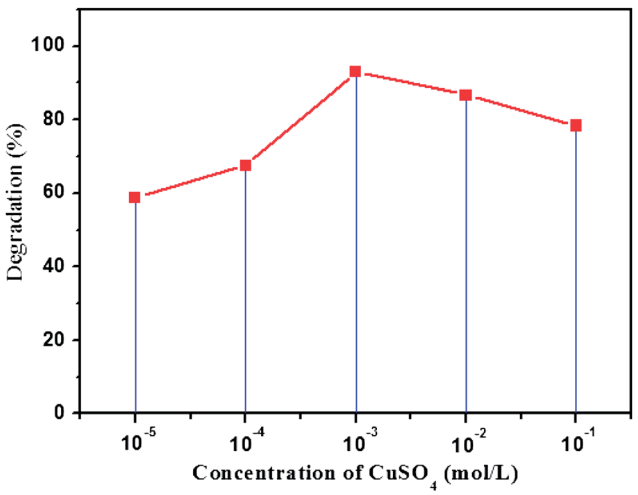

Fig. 9 Effect of concentration of the precursor $CuSO_4$ used to prepare paper–TiO_2–Cu_2O on the photodegradation of toluidine after 6 h of irradiation.

3.8. Reusability of the photocatalyst

The reusability of the paper–TiO_2–Cu_2O photocatalyst was tested repeatedly for four times. After each run the catalyst was rinsed with water, dried and used again in the same conditions. As shown in Fig. 10 the photodegradation efficiency of toluidine was still high enough even after four runs. Indeed, the photocatalytic performance of paper–TiO_2–Cu_2O toward toluidine degradation decreased gradually after each run but kept higher than 85% after four runs of sunlight irradiation. The gradual decrease in the photodegradation efficiency of toluidine with the reuse of the photocatalystis common for most TiO_2 based photocatalysts is attributed to the accumulation of the by-products on the active surface sites of the photocatalyst.[25] Specifically, for Cu_2O based photocatalyst, the reusability of the catalyst is hampered by the photocorrosion in an aqueous solution during illumination because the redox potential for the reduction and oxidation of Cu_2O lies within the band gap.[26] The maintenance of a good photocatalytic activity for the paper–TiO_2–Cu_2O photocatalyst is indicative that the photocorrosion of Cu_2O can be inhibited by coupling with TiO_2.

3.9. Binding efficiency of the catalyst layer on the paper

To confirm the efficient binding of TiO_2 layer on paper, an ultrasonication treatment on an ultrasonic bath (Power 50 W) was applied to paper–TiO_2–Cu_2O for 15 and 30 min, and the treated paper was characterized by Raman. No evolution on the aspect nor on the mechanical integrity of the paper was observed after the ultrasonication treatment and the Raman spectra (Fig. 11(I)) indicated the persistence of the TiO_2 band with a similar intensity than that of the neat paper–TiO_2–Cu_2O. This gives a sound evidence for the chemical binding of the TiO_2 layer on the surface of the paper and the efficient adhesion of Cu_2O NPs on TiO_2 layer. Presumably, the chemical binding of TiO_2 NPs on paper took place *via* chemical condensation of Ti–OH groups, formed during hydrothermal treatment, with the hydroxyl groups of the cellulose fibres of

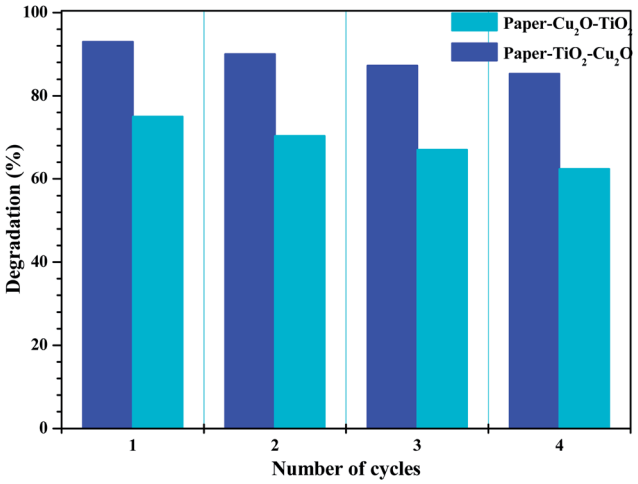

Fig. 10 Evolution of the degradation efficiency of paper–TiO_2–Cu_2O and paper–Cu_2O–TiO_2 after four degradation cycles of 6 h irradiation under sun light simulator.

paper. Moreover, the ultrasonication treatment did not led to any change in the photocatalytic activity of the hybrid photocatalyst (Fig. 11(II)). The evolution of the concentration of the residual toluidine followed nearly the same trend for the original paper–TiO_2–Cu_2O as well as for the paper–TiO_2–Cu_2O sonicated paper, confirming again the efficient binding of the catalyst layer onto the surface of the paper. In addition, the paper–TiO_2–Cu_2O did not show any sign of disintegration nor weakness after ultrasonication and prolonged contact with water.

3.10. Possible visible light-induced photocatalytic mechanism

The photocatalytic activity under visible light of the hybrid paper–TiO_2–Cu_2O or paper–Cu_2O–TiO_2 could be a result of a strong coupling between TiO_2 and Cu_2O which facilitated the interfacial charge transfer. This intimate contact between the two semi-conductors is the result of the synthesis method adopted in the present work. Indeed, since Cu_2O is generated *in situ* after adsorption of Cu^{2+} on the surface of TiO_2 layer, then a strong and intimate coupling between TiO_2 and Cu_2O is expected, favouring the formation of numerous p–n heterojunctions. Once the crystallization of TiO_2 took place after the hydrothermal treatment, we infer that the titania thin layer becomes in good contact with the underneath Cu_2O NPs. Under visible irradiation, the photoexcited electrons in the conduction band of Cu_2O are transferred to the conduction band of TiO_2, at the Cu_2O–TiO_2 interface, while the photoexcited holes in the valence band of TiO_2 should transfer to the valence band of Cu_2O. This transfer is made possible by the lower position of the conduction and valence bands of TiO_2 compared to those of Cu_2O. Indeed the band gaps of TiO_2 and Cu_2O are about 3.2 and 2.1 eV with the CB at −0.2 and −1.4 eV and the VB at 3 and 0.7 eV, respectively, compared with normal hydrogen electrode (NHE). The excess electrons on TiO_2 are trapped by chemisorbed molecular oxygen to produce the

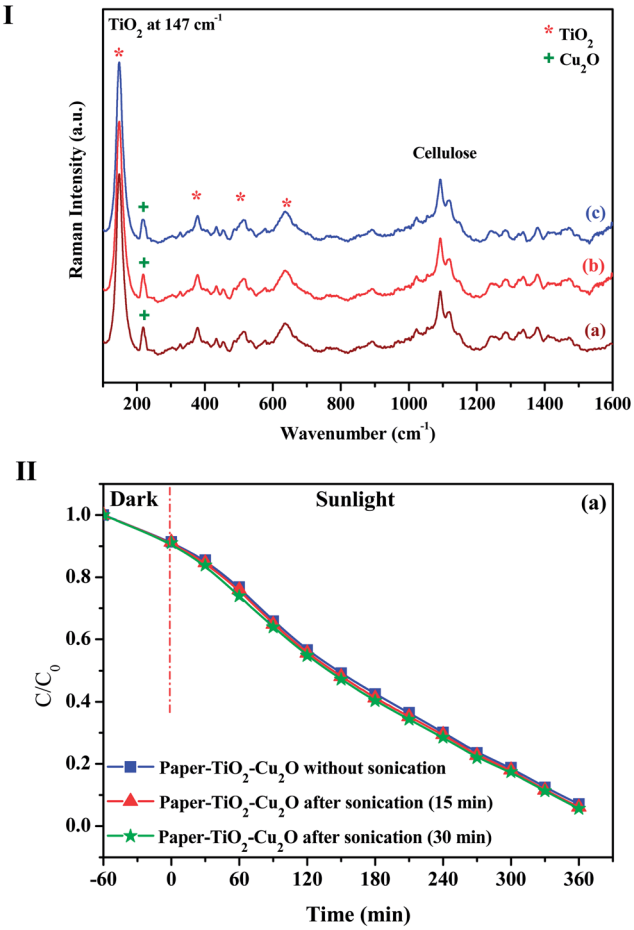

Fig. 11 (I) Raman spectra of paper–TiO_2–Cu_2O: prior to ultrasonication (a) and after ultra sonication, during 15 min (b) 30 min (c), (II) time dependence of the residual concentration of toluidine for paper–TiO_2–Cu_2O prior and after ultrasonication during 15 and 30 min.

superoxide radical anion and the holes in the VB of Cu_2O could react with adsorbed H_2O or OH^- species to produce highly reactive $^{\bullet}OH$ radicals in aqueous solution. These reactive oxidizing groups would react with organic pollutants to accomplish degradation.

The whole process can be clearly described as follows:

$$TiO_2\text{–}Cu_2O \text{ or } Cu_2O\text{–}TiO_2 + h\nu \rightarrow Cu_2O\,(h_{VB}^{+}) + TiO_2\,(e_{CB}^{-}) \quad (2)$$

$$TiO_2\,(e^-) + O_2 \rightarrow TiO_2 + {}^{-}O_2^{\bullet} \quad (3)$$

$$Cu_2O\,(h^+) + OH^- \rightarrow Cu_2O + {}^{\bullet}OH \quad (4)$$

$$Cu_2O\,(h^+) + H_2O \rightarrow Cu_2O + H^+ + {}^{\bullet}OH \quad (5)$$

$$\text{Organic pollutant} + {}^{\bullet}OH \rightarrow \text{degradation of organic pollutant} \quad (6)$$

A schematic illustration of effective separation and instant scavenging of photoexcited electron–hole pairs in TiO_2–Cu_2O and Cu_2O–TiO_2 is presented in Scheme 2.

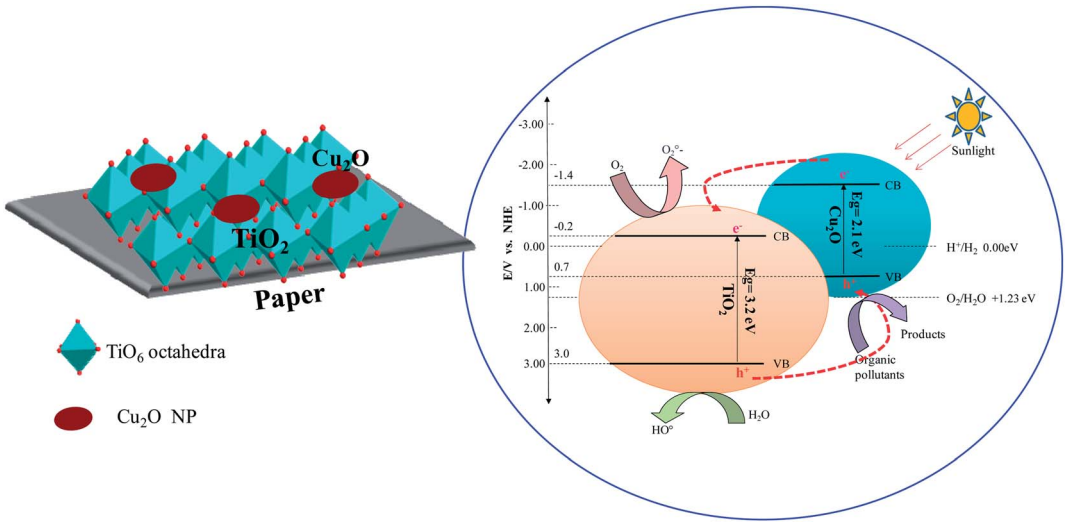

Scheme 2 Schematic illustration of effective separation and instant scavenging of photoexcited electron–hole pairs in TiO_2–Cu_2O and Cu_2O–TiO_2.

4. Conclusions

An environmental friendly approach to prepare paper–TiO_2, paper–TiO_2–Cu_2O and paper–Cu_2O–TiO_2 hybrid catalyst was discussed. The TiO_2 phase in the form of anatase, as confirmed by Raman, formed a thin homogeneous layer composed by tiny NPs with a size lower than 10 nm as revealed by and FE-SEM observation. The Cu_2O phase was in the form of NPs with 30 to 100 nm in size dispersed over the surface of the paper/or over the TiO_2 layer. The presence of Cu_2O NPs extended the light adsorption in the visible up to 500 nm. However, the red shift in the absorption was more pronounced for paper–TiO_2–Cu_2O than paper–Cu_2O–TiO_2. The hybrid paper–TiO_2, paper–TiO_2–Cu_2O and paper–Cu_2O–TiO_2 catalysts were applied in the degradation of the toluidine in water under exposition to simulated sunlight. The degradation efficiency was affected by the presence of Cu_2O NPs and increased from 30% for paper–TiO_2 to 75 and 93% for paper–Cu_2O–TiO_2 and paper–TiO_2–Cu_2O, respectively after 6 h of exposition to sun-light stimulant. The photocatalyst was reusable for several degradation cycles with only small reduction in the degradation efficiency and without disintegration of the paper. This advantage is important in the continuous photocatalytic degradation process. The preparation technique of the hybrid paper–TiO_2–Cu_2O catalyst is reliable, economic, easy to implement and may be applied to any type of paper. Best to our knowledge, it is the first work reporting the preparation, characterization and the application of hybrid paper–TiO_2–Cu_2O as photocatalyst.

References

1 D. Robert, A. Piscopo, O. Heintz and J.-V. Weber, *Catal. Today*, 1999, **54**, 291–296.
2 B. Li, J. M. Wu, T. T. Guo, M. Z. Tang and W. Wen, *Nanoscale*, 2014, **6**, 3046.
3 S. Sakthivel, M. V. Shankar, M. Palanichamy, B. Arabindoo and V. J. Murugesan, *J. Photochem. Photobiol., A*, 2002, **148**, 153–159.
4 S. Yao, J. Li and Z. Shi, *Particuology*, 2010, **8**, 272–278.
5 M. Abid, S. Bouattour, D. S. Conceição, A. M. Ferraria, L. F. Vieira Ferreira, A. M. Botelho do Rego, M. Rei Vilar and S. Boufi, *RSC Adv.*, 2016, **6**, 58957–58969.
6 C.-S. Kim, I.-M. Kwon, B. K. Moon, J. H. Jeong, B.-C. Choi, J. H. Kim, H. Choi, S. S. Yi, D.-H. Yoo, K.-S. Hong, J.-H. Park and H. S. Lee, *Mater. Sci. Eng., C*, 2007, **27**, 1343–1346.
7 M. J. Uddin, F. Cesano, F. Bonino, S. Bordiga, G. Spoto, D. Scarano and A. J. Zecchina, *J. Photochem. Photobiol., A*, 2007, **189**, 286–294.
8 W. A. Daoud and J. H. Xin, *J. Am. Ceram. Soc.*, 2004, **87**(5), 953–955.
9 H. Matsubara, M. Takad, S. H. Koyama, K. Hashimoto and A. Fujishima, *Chem. Lett.*, 1995, **9**, 767–768.
10 Y. Iguchi, H. Ichiura, T. Kitaoka and H. Tanaka, *Chemosphere*, 2003, **53**, 1193–1199.
11 M. Kemell, V. Pore, M. Ritala, M. Leskelä and M. Lindén, *J. Am. Chem. Soc.*, 2005, **127**, 14178–14179.
12 R. Pelton, X. Geng and M. Brook, *Adv. Colloid Interface Sci.*, 2006, **127**, 43–53.
13 M. Y. Shen, T. Yokouchi, S. S. Koyama and T. Goto, *Phys. Rev. B: Condens. Matter Mater. Phys.*, 1997, **56**, 13066–13072.
14 Y. Bessekhouad, D. Robert and J.-V. Weber, *Catal. Today*, 2005, **101**, 315–321.
15 J. Y. Ho and M. H. Huang, *J. Phys. Chem. C*, 2009, **113**, 14159–14164.
16 D. A. Shirley, *Phys. Rev. B: Solid State*, 1972, **5**, 4709–4713.
17 T. Ohsaka, F. Izumi and Y. Fujiki, *J. Raman Spectrosc.*, 1978, **7**, 321–324.
18 L. L. Lai, W. Wen and J. M. Wu, *CrystEngComm*, 2016, **18**, 5195.

19 A. Errokh, A. M. Ferraria, D. S. Conceicã, L. F. Vieira Ferreira, A. M. Botelho do Rego, M. Rei Vilar and S. Boufi, *Carbohydr. Polym.*, 2016, **141**, 229–237.
20 N. Riaz, F. K. Chong, B. K. Dutta, Z. B. Man, M. S. Khan and E. Nurlaela, *Chem. Eng. J.*, 2012, **185**, 108–119.
21 J. M. Wu and B. Qi, *J. Am. Ceram. Soc.*, 2008, **91**, 3961.
22 L. Liu, W. Yang, W. Sun, Q. Li and J. K. Shang, *ACS Appl. Mater. Interfaces*, 2015, **7**, 1465–1476.
23 A. Ajmal, I. Majeed, R. N. Malik, M. Iqbal, M. Arif Nadeem, I. Hussain, S. Y. Zeshan, G. Mustafa, M. I. Zafar and M. Amtiaz Nadeem, *J. Environ. Chem. Eng.*, 2016, **4**, 2138–2146.
24 S. Song, R. Rao, H. Yang and A. Zhang, *J. Phys. Chem. C*, 2010, **114**, 13998–14003.
25 A. Hamdi, S. Boufi and S. Bouattour, *Appl. Surf. Sci.*, 2015, **339**, 128–136.
26 A. Paracchino, V. Laporte, K. Sivula, M. Grätzel and E. Thimsen, *Nat. Mater.*, 2011, **10**, 456–461.